CELL BIOLOGY

Astrocytic lipid metabolism determines susceptibility to diet-induced obesity

Luis Varela[1,2]*, Jae Geun Kim[3], Pablo Fernández-Tussy[1,4], Binod Aryal[1,4], Zhong Wu Liu[1,2], Carlos Fernández-Hernando[1,2,4], Tamas L. Horvath[1,2]*

Hypothalamic astrocytes play pivotal roles in both nutrient sensing and the modulation of synaptic plasticity of hypothalamic neuronal circuits in control of feeding and systemic glucose and energy metabolism. Here, we show the relevance of astrocytic fatty acid (FA) homeostasis under the opposing control of angiopoietin-like 4 (ANGPTL-4) and peroxisome proliferator–activated receptor gamma (PPARγ) in the cellular adaptations of hypothalamic astrocytes and neurons to the changing metabolic milieu. We observed that increased availability of FA in astrocytes induced by cell- and time-selective knockdown of *Angptl4* protected against diet-induced obesity, while cell- and time-selective knockdown of *Angptl4*-regulated *Pparγ* lead to elevated susceptibility to obesity. Overall, our results unravel a previously unidentified role for astrocytic FA metabolism in central control of body weight and glucose homeostasis.

INTRODUCTION

Once considered merely supportive cells (*1*), astrocytes have emerged as key players in the regulation of brain functions and the onset of different diseases, including Alzheimer's disease and schizophrenia (*2*–*4*). The role of astrocytes has also recently been identified in hypothalamic control of energy balance (*5*–*9*). For example, we have shown that hypothalamic astrocytes are associated with synaptic plasticity of critical hypothalamic neuronal circuits involved in control of feeding and glucose metabolism (*6*), a process that we recently showed to be actively involved with controlled synapse removal (*10*).

A number of studies have reported on lipid metabolism in the hypothalamus (*11*–*14*). Response to different metabolic challenges can modulate the expression of genes involved in de novo lipogenesis or lipid transport in the hypothalamus. While a subpopulation of neurons within the hypothalamus were shown to use fatty acid (FA) as fuel in situations of low glucose availability (*15*), it is thought that neurons have a reduced capacity of FA oxidation in support of their normal function (*16*). Contrary to this, astrocytes are the main site of FA β-oxidation within the central nervous system (CNS) (*16*, *17*). In periods of elevated fuel requirement or low glucose availability, these cells can use alternative fuels. It is estimated that about 20% of all the energy required for maintenance of basal activity of the brain is provided by FA (*16*).

Changes in systemic nutritional status can substantially alter nutrient availability in the bloodstream and thereby modulate special fuel availability for astrocytes. How these alterations in fuel availability of astrocytes may affect central neuronal circuits and related behavioral and autonomic output is ill-defined. This study was undertaken to interrogate this question by genetic manipulation of FA availability in astrocytes.

Mitochondrial dynamics have been widely studied in many systems, organs, and CNS areas and cell types (*18*–*22*). From the different factors that have been shown to affect mitochondria morphology (neuronal activation, cell death, or innate immunity), fuel utilization is gaining relevance due to its ease to trigger fusion-fission events (*18*–*20*). Studies in cell cultures have described how exposure of cells to changing concentrations of different nutrients can rapidly modulate mitochondria size, number, or shape; treatments with FA trigger mitochondrial fission or fragmentation leading to smaller and more rounded mitochondria (*23*–*25*). On the other hand, glucose administration induces fusion leading to bigger and more elongated mitochondria (*8*, *24*, *26*).

Angiopoietin-like 4 (ANGPTL4) was originally identified as a peroxisome proliferator–activated receptor gamma (PPARγ)–responsive gene highly expressed in adipose tissues and liver, as well as, to a lesser extent, in heart, muscle, and other tissues (*27*). Its expression is tightly regulated by nutritional and metabolic state, and ANGPTL4 controls FA availability to different tissues by suppressing the activity of lipoprotein lipase (LPL), the enzyme that hydrolyze triglycerides (TGs) into glycerol and FA (*28*, *29*). The physiologic relevance of hepatic and adipose tissue–derived ANGPTL4 in regulating lipoprotein catabolism, obesity, insulin resistance, and atherosclerosis has been recently elucidated (*30*–*32*). However, the specific contribution of ANGPTL4 in the CNS, and particularly in astrocytes, a glial cell where ANGPTL4 is mainly expressed (*33*, *34*), in regulating systemic metabolism remains unknown.

Here, we show that astrocyte-specific ablation of angiopoietin-like 4 (*Angptl4*) in adult mice prevented high-fat diet (HFD)–induced adaptations of hypothalamic astrocytes and neurons and protected against diet-induced obesity while increasing hypothalamic *Pparγ* mRNA levels. Conversely, astrocyte-specific deletion of *Pparγ* exacerbated the susceptibility to HFD, leading to altered hypothalamic circuit integrity, a hyperphagic phenotype, and increased body weight.

RESULTS

Astrocytic mitochondrial adaptations during diet-induced obesity

We previously reported that, in hypothalamic neurons, mitochondria dynamics are affected by systemic energetic status (*19*, *20*, *35*).

[1]Department of Comparative Medicine, Yale University School of Medicine, 310 Cedar St., BML 330, New Haven, CT 06520, USA. [2]Yale Center for Molecular and Systems Metabolism, Yale University School of Medicine, 310 Cedar St., BML 330, New Haven, CT 06520, USA. [3]Division of Life Sciences, College of Life Sciences and Bioengineering, Incheon National University, Incheon 406-772, South Korea. [4]Vascular Biology and Therapeutics Program, School of Medicine, Yale University, New Haven, CT 06510, USA.
*Corresponding author. Email: luis.varela@yale.edu (L.V.); tamas.horvath@yale.edu (T.L.H.)

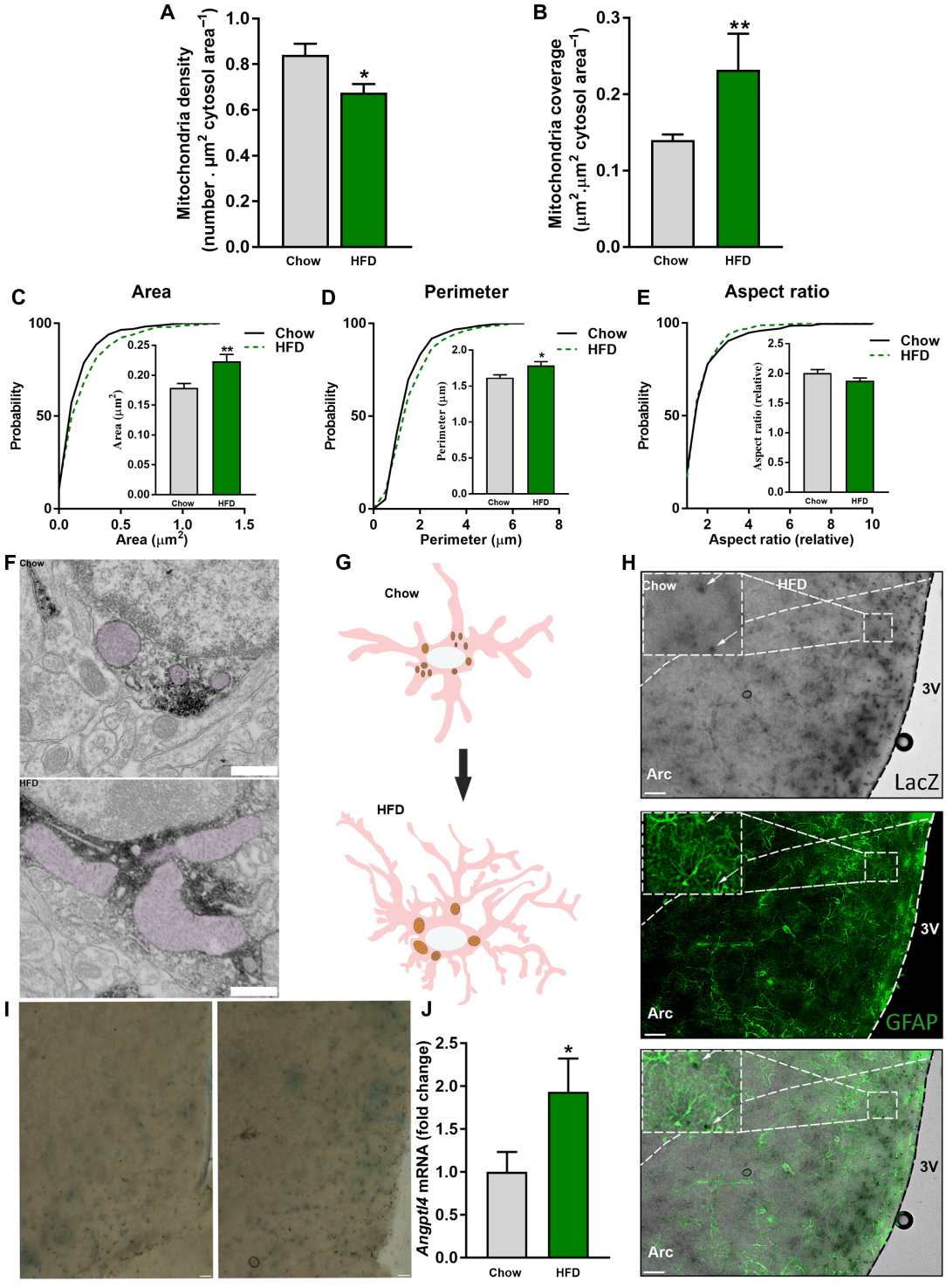

Fig. 1. HFD induces changes in astrocytic mitochondrial morphology. Mitochondria (**A**) density and (**B**) coverage in MBH astrocytes of mice exposed to chow and HFD. Cumulative distribution and mean of mitochondria (**C**) area, (**D**) perimeter, and (**E**) aspect ratio of mediobasal hypothalamus (MBH) astrocytes of mice fed a chow diet and HFD ($n > 350$ mitochondria from >43 astrocytes from 12 and 9 mice, respectively). (**F**) Representative electron micrographs from MBH astrocytes of mice fed a chow diet and HFD. Scale bar, 500 nm. (**G**) Schematic representation of astrocytes and their mitochondria in response to HFD feeding. (**H**) Representative images showing colocalization of glial fibrillary acidic protein (GFAP) and ANGPTL4-LacZ. Scale bars, 100 µm. (**I**) Representative images showing ANGPTL4-LacZ staining in the MBH of chow- and HFD-fed mice. Scale bars, 50 µm. (**J**) *Angptl4* mRNA levels from MBH astrocytes of mice fed a chow diet and HFD ($n = 6$ and 7 samples per group, respectively). Data are presented as means ± SEM. $^{*}P \leq 0.05$, and $^{***}P \leq 0.001$ as determined by two-tailed *t* test or Kolmogorov-Smirnov test for analyses of cumulative distribution.

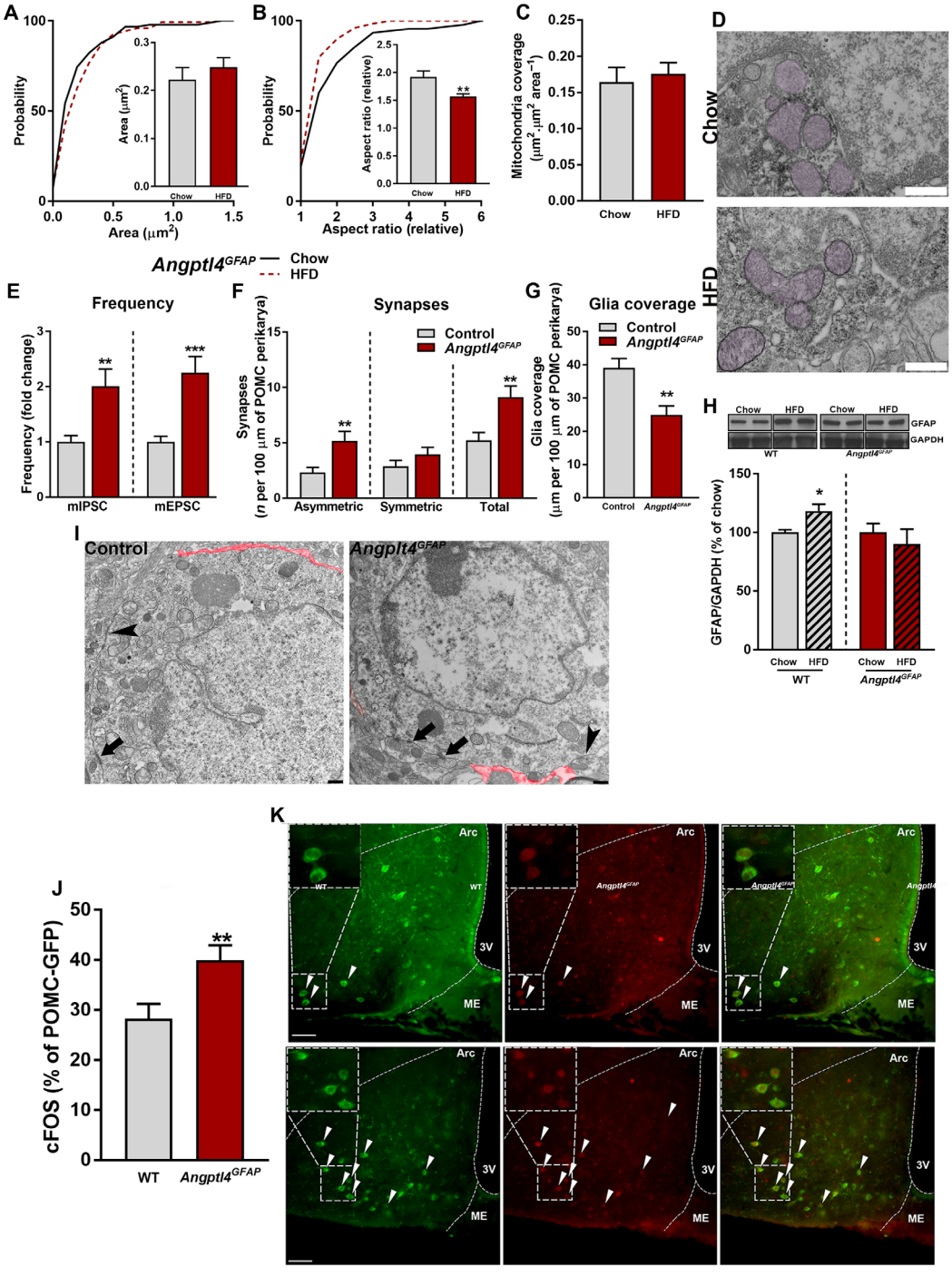

Fig. 2. Loss of astrocytic ANGPTL4 impairs mitochondrial adaptive responses during chronic exposure to HFD. Cumulative distribution and mean of mitochondria (**A**) area, (**B**) aspect ratio, and (**C**) mean of mitochondria coverage of MBH astrocytes of *Angptl4*^{GFAP} mice exposed to chow and HFD ($n > 90$ mitochondria from >12 astrocytes from four and five mice per group, respectively). (**D**) Representative electron micrographs from MBH astrocytes of *Angptl4*^{GFAP} mice exposed to chow and HFD. Scale bar, 500 nm. (**E**) Electrophysiological recordings showing frequency of miniature inhibitory postsynaptic currents (mIPSC) and from *Angptl4*^{GFAP} mice and their controls exposed to HFD ($n = 27$ and 28 POMC cells from four mice per group, respectively). GAPDH, glyceraldehyde-3-phosphate dehydrogenase. (**F**) Number of synapses per 100 μm of POMC perikarya and (**G**) glia coverage in mice *Angptl4*^{GFAP} and their controls after HFD feeding ($n = 15$ and 18 neurons from four or five mice per group, respectively). (**H**) Quantification and representative blots [from the same film (chow versus HFD)] showing the levels of GFAP in the MBH of *Angptl4*^{GFAP} mice and their controls on chow and HFD ($n > 5$ mice per group). WT, wild-type. (**I**) Representative electron micrographs showing glia coverage and synaptic events onto the POMC perikarya of *Angptl4*^{GFAP} mice and their control littermates fed an HFD. Red trace illustrates glia coverage. Arrowheads depict symmetric synapses. Arrows depict asymmetric synapses. Scale bar, 500 nm. GFP, green fluorescent protein. (**J**) Percentage of activated POMC neurons and (**K**) representative confocal images showing cFOS (red) and POMC neurons (green) of *Angptl4*^{GFAP} mice and their controls during HFD feeding ($n = 27$ or 28 sections from 4 and 5 mice per group, respectively). Arrowheads denote colocalization between cFOS and POMC. ME, median eminence; 3V, third ventricle. Scale bar, 50 μm. Data are presented as means ± SEM. $^{*}P \leq 0.05$, $^{**}P \leq 0.01$, and $^{***}P \leq 0.001$ as determined by two-tailed *t* test or Kolmogorov-Smirnov test for analyses of cumulative distribution.

The impact of nutrient availability on mitochondria of hypothalamic astrocytes is less explored. Here, we interrogated whether mitochondrial parameters are affected in hypothalamic astrocytes in response to HFD feeding. We found that chronic exposure of mice to HFD induced significant changes in different mitochondria parameters, including reduced number and larger size in hypothalamic astrocytes (Fig. 1, A to G).

The absence of astrocytic *Angptl4* affects mitochondria network and protects against diet-induced obesity

There are various ways via which HFD can affect hypothalamic astrocytes. For example, TG may affect these cells by the mediation on LPL. LPL is a "gatekeeper" for FA delivery in peripheral tissues. LPL is also expressed in astrocytes, and its absence decreased lipid accumulation and exacerbated diet-induced obesity (*5*). We found that ANGPTL4, an inhibitor of LPL (*28*, *29*, *32*–*34*, *36*–*39*), is highly expressed in the mediobasal hypothalamus (MBH), and its expression is up-regulated by HFD exposure (Fig. 1, H to J, and fig. S1, A to C). To interrogate the role of ANGPTL4 in HFD-induced adaptations of astrocytic mitochondria, we generated astrocyte-specific ANGPTL4 knockout mice (hereafter, $Angptl4^{GFAP}$) (figs. S1, D to G; S2, A to I; and S3). Whereas $Angptl4^{GFAP}$ mice eating a chow diet did not show significant changes in most of the studied parameters and only displayed ameliorated glucose clearance (fig. S2E), we found that they responded strongly to HFD exposure. We observed that, in contrast to controls (Fig. 1, A to G), HFD did not evoke changes in the morphology of astrocytic mitochondria in $Angptl4^{GFAP}$ mice (Fig. 2, A to D).

We have previously shown that hypothalamic astrocytes are involved in the adaptive synaptic changes on hypothalamic, anorexigenic proopiomelanocortin (POMC) perikaryal with systemic metabolic impact (*6*, *7*). Thus, we investigated whether the changes in astrocytic mitochondria described above have an impact on POMC neuronal input organization and activity. By using electron microscopy and electrophysiology, we found that $Angptl4^{GFAP}$ mice showed an increased number of POMC perikaryal synapses, which were due to increased number of asymmetric, putative excitatory synapses (Fig. 2, E, F, and I). In addition, while HFD induced increased glial ensheetment of POMC perikaryal in control mice (Fig. 2, G to I), these changes did not occur on POMC neurons of $Angptl4^{GFAP}$ mice (Fig. 2, G to I). These changes in perikaryal input organization of POMC neurons were paralleled by significantly higher activation of POMC neurons in $Angptl4^{GFAP}$ mice as assessed by cFOS expression (Fig. 2, J and K).

In line with increased excitability of POMC neurons of $Angptl4^{GFAP}$ mice, these animals showed a lean and hypophagic phenotype when exposed to HFD (Fig. 3, A to E, and fig. S4). Astrocyte-specific deficient ANGPTL4 mice also showed improved glucose tolerance and enhanced insulin sensitivity during diet-induced obesity (Fig. 3, F and G). The absence of phenotype in $Angptl4^{GFAP}$ mice is likely due to the necessity of changes in the fuel availability that impacts astrocytic mitochondria function. Overall, these results demonstrated a crucial contribution of astrocytic ANGPTL4 in controlling hypothalamic astrocytic and neuronal circuit adaptations during HFD feeding.

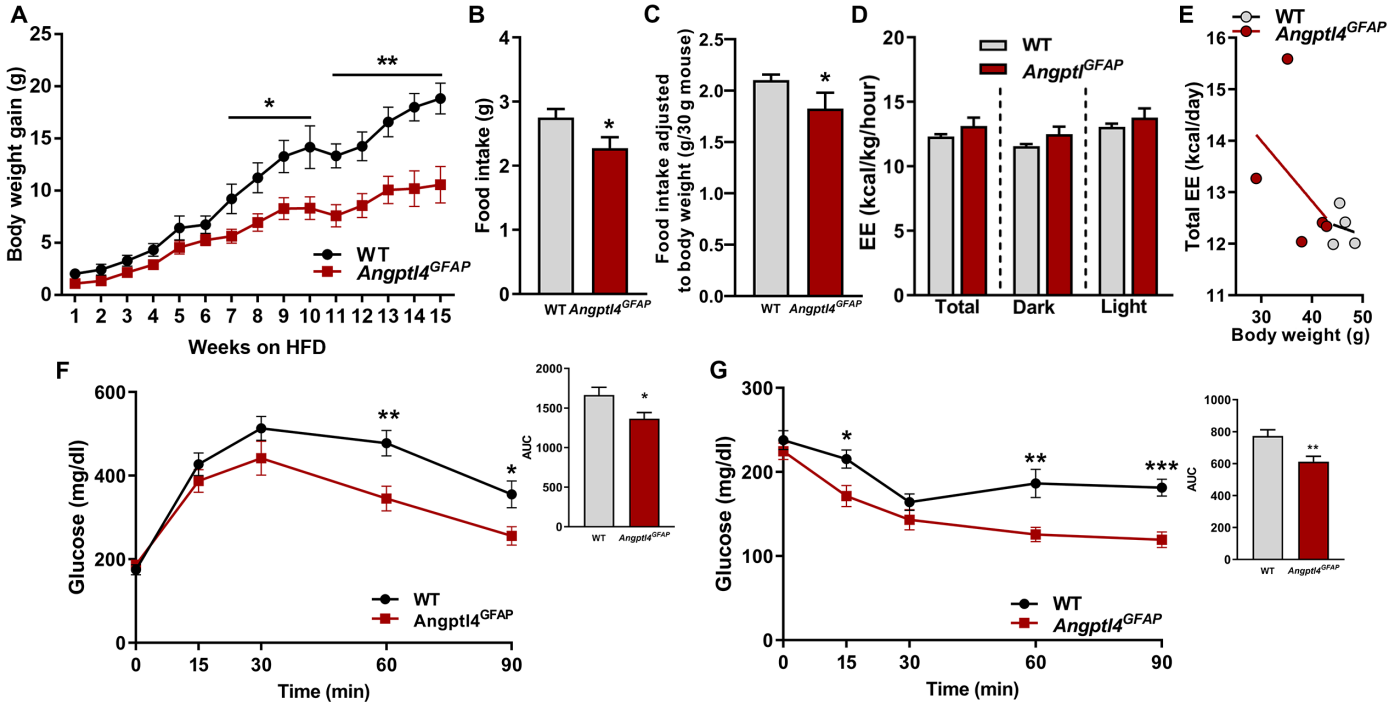

Fig. 3. Loss of astrocytic ANGPTL4 impairs body weight gain during chronic exposure to HFD. (**A**) Body weight gain, (**B**) daily food intake, (**C**) food intake adjusted to the body weight, and (**D** and **E**) energy expenditure (EE) of $Angptl4^{GFAP}$ mice and their controls during HFD intervention. (**F**) Glucose tolerance test (GTT) and area under curve (AUC) and (**G**) insulin tolerance test (ITT) and AUC in $Angptl4^{GFAP}$ mice and their controls during HFD feeding ($n = 8$ and 7 mice per group, respectively). Data are presented as means ± SEM. $^{*}P \leq 0.05$, $^{**}P \leq 0.01$, and $^{***}P \leq 0.001$ as determined by two-tailed *t* test.

Angptl4 regulates *Pparγ* expression in astrocytes

PPARγ is a nuclear receptor that controls the expression of genes involved in lipid metabolism and transport (*40*, *41*). Notably, we found an inverse correlation between the expression of ANGPTL4 and PPARγ in the MBH in response to changes in the energetic status (Fig. 4A). We also observed that *Angptl4*^{GFAP} mice had increased levels of PPARγ in the MBH (Fig. 4B), suggesting that the observed cellular, circuit, and systemic alterations we found may be due to PPARγ-mediated events. To interrogate this, we generated astrocyte-specific PPARγ knockout mouse (hereafter, *Ppar*^{GFAP}) (figs. S2, J to O, and S5).

Loss of astrocytic *Pparγ* increases susceptibility to HFD while affecting mitochondrial dynamics

In support of the regulatory relationship between ANGPTL4 and PPARγ, *Ppar*^{GFAP} mice showed the opposite phenotype as *Angptl4*^{GFAP} mice; whereas *Angptl4*^{GFAP} animals showed increased LPL activity in diverse areas of the brain and the up-regulation of different proteins involved in lipid metabolism in the MBH (Fig. 4, C to E), *Ppar*^{GFAP} mice presented reduced expression of genes involved in lipid metabolism and transport (Fig. 4, F to H). Notably, the expression of *Cd36*, a plasma membrane FA transporter, was significantly attenuated in hypothalamic astrocytes from *Ppar*^{GFAP} mice compared

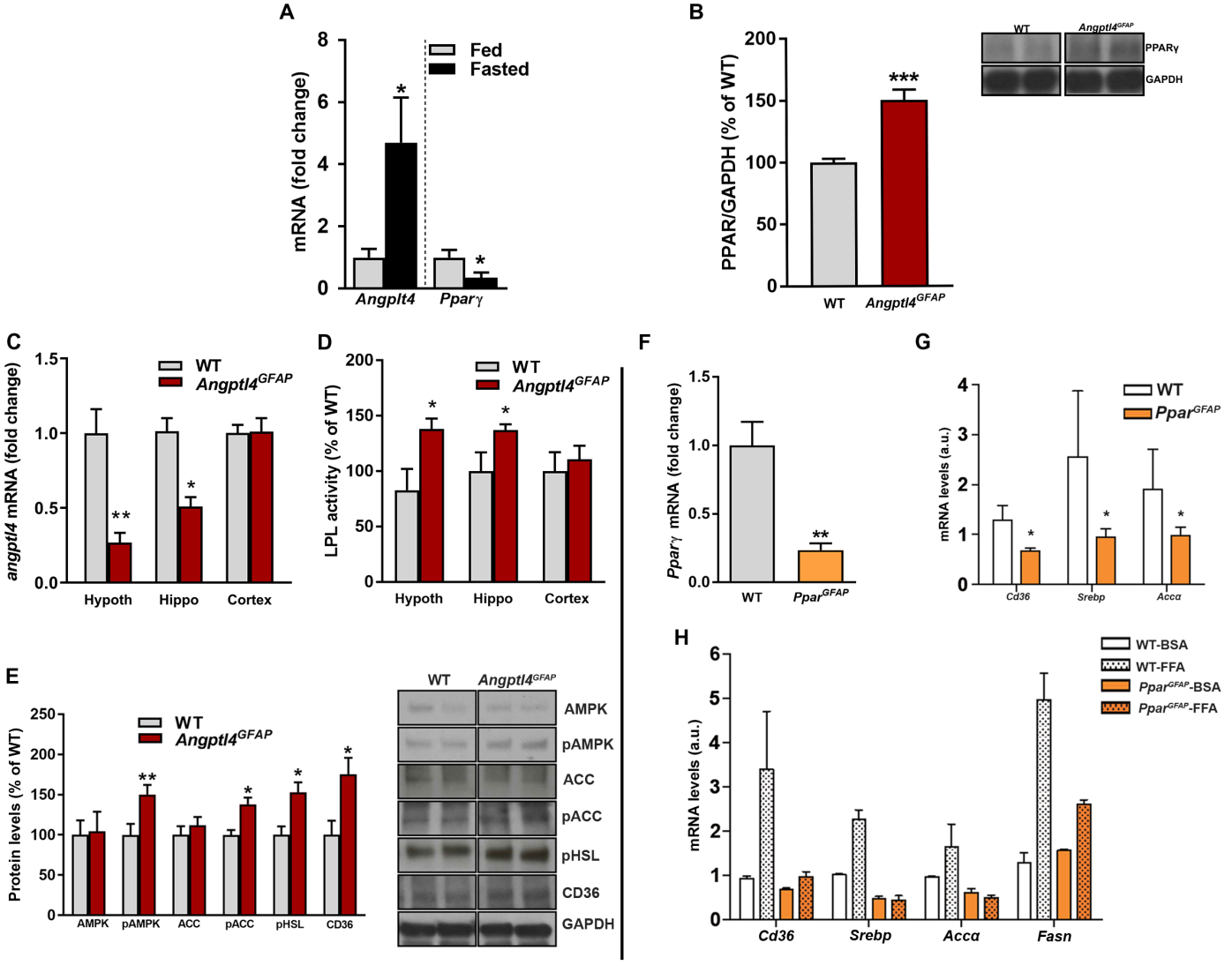

Fig. 4. ANGPTL4 regulates the expression of PPARγ. (**A**) *Angptl4* and *Pparγ* mRNA levels from hypothalamic astrocytes of fed and fasted WT mice ($n = 4$ mice per group). (**B**) Quantification and representative blots (from the same film) showing the levels of PPARγ in MBH of *Angptl4*^{GFAP} mice and their littermate controls ($n = 5$ mice per group). (**C**) *Angptl4* mRNA levels and (**D**) LPL activity in the hypothalamus, hippocampus, and cortex of *Angptl4*^{GFAP} mice and their controls ($n > 7$ mice per group). (**E**) Quantification and representative blots (from the same film) showing the levels of AMPK (AMP-activated protein kinase), pAMPK, ACC (acetyl-CoA carboxylase), pACC, pHSL (phosphorylated hormone-sensitive lipase), and CD36 in the MBH of *Angptl4*^{GFAP} mice and their controls ($n = 5$ mice per group). (**F**) *Pparγ* mRNA levels from hypothalamic astrocytes of *Ppar*^{GFAP} mice and their controls ($n = 4$ samples per group). (**G**) *Cd36*, *Srebp*, and *Acc* mRNA levels from hypothalamic astrocytes of *Ppar*^{GFAP} and their control mice ($n = 4$ samples per group). a.u., arbitrary units. (**H**) *Cd36*, *Srebp*, *Acc*, and *Fasn* mRNA levels from primary cultures of hypothalamic astrocytes of *Ppar*^{GFAP} and their control mice treated with bovine serum albumin (BSA) or free fatty acid (FFA) ($n = 4$ or 5 samples per group). Data are presented as means ± SEM. $^{*}P \leq 0.05$, $^{**}P \leq 0.01$, and $^{***}P \leq 0.001$ as determined by two-tailed *t* test.

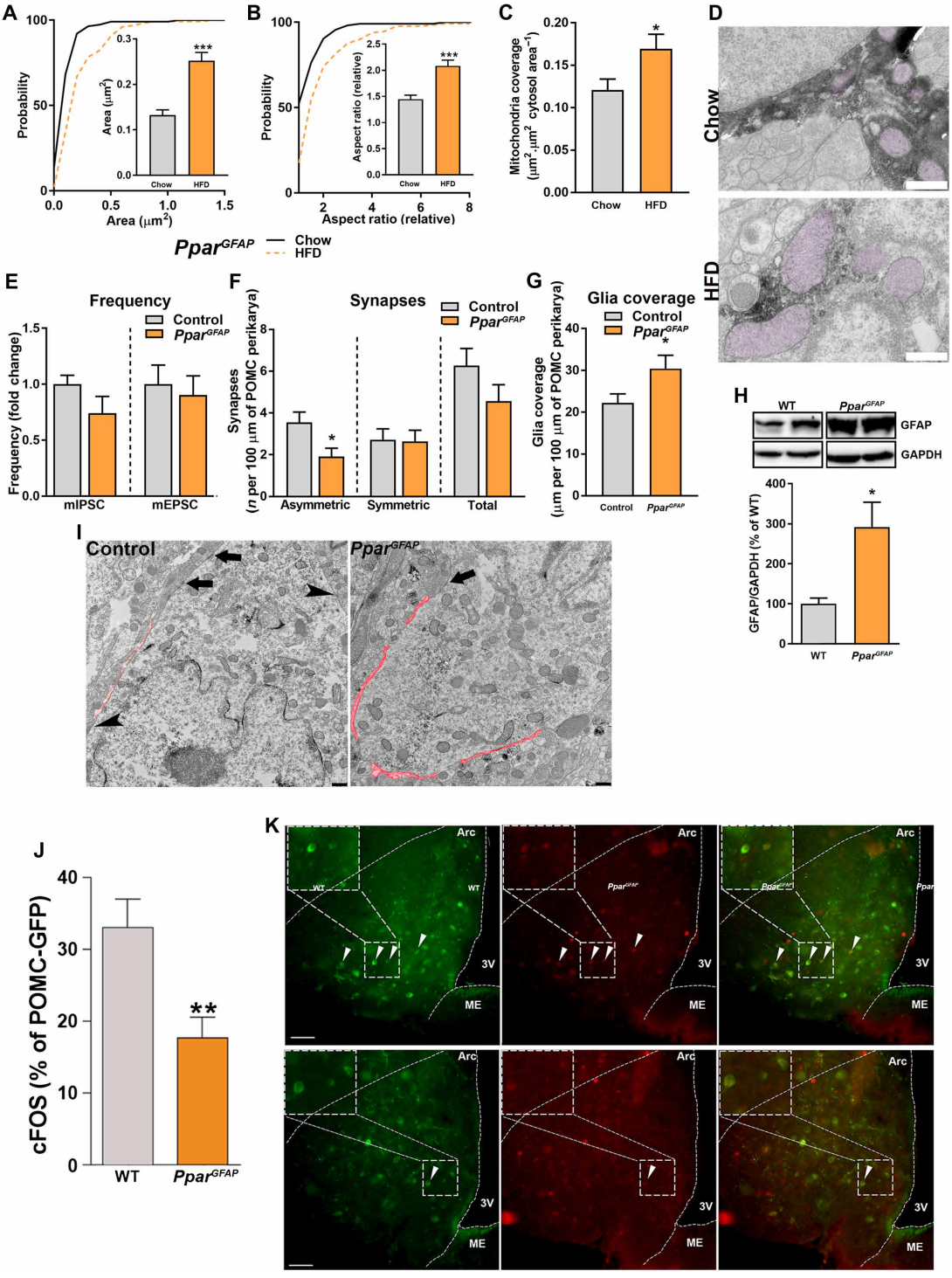

Fig. 5. Loss of astrocytic PPARγ exacerbates the mitochondrial adaptations to chronic exposure to HFD. Cumulative distribution and mean of mitochondria (**A**) area, (**B**) aspect ratio, and (**C**) mean of mitochondria coverage of MBH astrocytes of *Ppar*^{GFAP} mice exposed to chow and HFD ($n > 130$ mitochondria from >13 astrocytes from four mice per group). (**D**) Representative electron micrographs from MBH astrocytes of *Ppar*^{GFAP} mice exposed to chow and HFD. Scale bar, 500 nm. (**E**) Electrophysiological recordings showing frequency of mIPSC and mEPSC from *Ppar*^{GFAP} mice and their controls exposed to HFD ($n > 12$ neurons from four mice per group). (**F**) Number of synapses and (**G**) glia coverage per 100 μm of POMC perikarya in mice *Ppar*^{GFAP} and their controls after HFD feeding ($n = 19$ and 15 neurons from four mice per group, respectively). (**H**) Quantification and representative blots (from the same film) showing the levels of GFAP in the MBH of *Ppar*^{GFAP} mice and their controls on chow and HFD ($n = 5$ and 6 mice per group, respectively). (**I**) Representative electron micrographs showing glia coverage and synaptic events onto the POMC perikarya of *Ppar*^{GFAP} mice and their control littermates fed a HFD. Red trace illustrates glia coverage. Arrowheads depict symmetric synapses. Arrows depict asymmetric synapses. Scale bar, 500 nm. (**J**) Percentage of activated POMC neurons and (**K**) representative confocal images showing cFOS (red) and POMC neurons (green) of *Ppar*^{GFAP} mice and their controls during HFD feeding. Arrowheads denote colocalization between cFOS and POMC. Scale bars, 50 μm. Data are presented as means ± SEM. *$P \leq 0.05$ and **$P \leq 0.01$ as determined by two-tailed *t* test or Kolmogorov-Smirnov test for analyses of cumulative distribution.

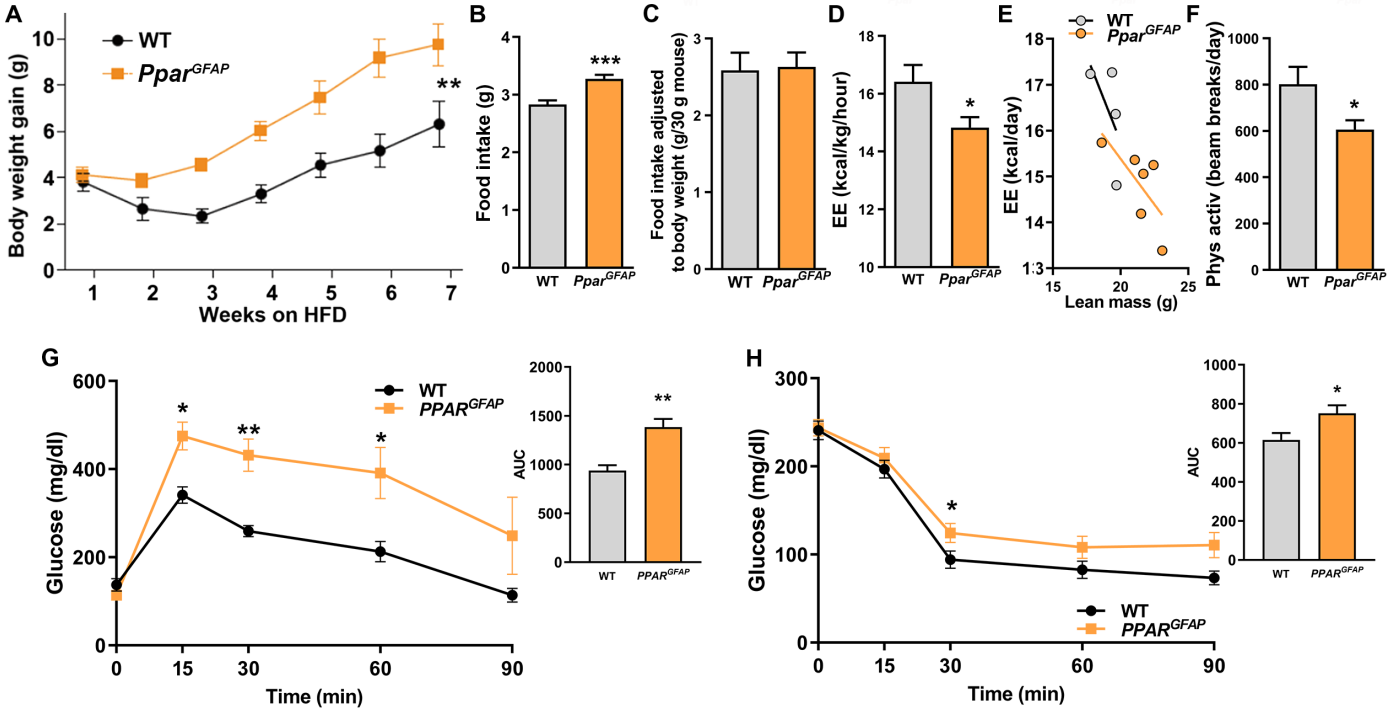

Fig. 6. Loss of astrocytic PPARγ exacerbates the metabolic susceptibility to chronic exposure to HFD. (**A**) Body weight gain, (**B**) food intake ($n = 7$ and 11 mice per group, respectively), (**C**) food intake adjusted to body weight, (**D** and **E**) energy expenditure, and (**F**) physical activity of $Ppar^{GFAP}$ mice and their controls during HFD intervention ($n = 4$ or 6 per group, respectively). (**G**) GTT and (**H**) ITT in $Ppar^{GFAP}$ mice and their controls during HFD feeding ($n > 4$ mice per group). Data are presented as means ± SEM. $^{*}P \leq 0.05$, $^{**}P \leq 0.01$, and $^{***}P \leq 0.001$ as determined by two-tailed *t* test or Kolmogorov-Smirnov test for analyses of cumulative distribution.

to wild-type (WT) mice (Fig. 4G). Astrocyte mitochondria analysis revealed significantly augmented changes in size and shape compared to control mice on HFD treatment (Fig. 5, A to D). We found that $Ppar^{GFAP}$ mice showed increased levels of glial fibrillary acidic protein (GFAP) in response to HFD exposure when compared to control mice (Fig. 5H). These changes were accompanied by an increased glial ensheetment of POMC cells (Fig. 5, G and I). Correspondingly, $Ppar^{GFAP}$ mice had lower number of synapses on POMC neuron perikaryal predominantly affecting asymmetrical, putative excitatory input (Fig. 5, E, F, and I). This increased putative inhibitory tone of POMC cells observed in $Ppar^{GFAP}$ mice resulted in diminished activation of these cells in response to HFD (Fig. 5, J and K).

The above changes in astrocytic mitochondria, cytoarchitecure, input organization, and activity of POMC neurons of $Ppar^{GFAP}$ mice lead to a hyperphagic and heavier phenotype (Fig. 6, A to F). These mice also exhibited impaired glucose clearance and insulin sensitivity and lowered energy expenditure when compared to WT mice fed an HFD (Fig. 6, G and H). The obese phenotype of $Ppar^{GFAP}$ mice on HFD was due not only to increased feeding but also to changes in energy expenditure and physical activity (Fig. 4, O to Q).

DISCUSSION

Hypothalamic lipid metabolism has been linked to the control of energy balance (*11*–*13*, *15*, *42*). Modulation of various lipid pathways in the hypothalamus has demonstrated their involvement in the maintenance of body weight and food intake by modulating the activity of peripheral organs. Despite its relevance, study of hypothalamic lipid metabolism has been focused on specific nucleus and neuronal populations, but it has not been well studied in other cell types (*5*). Astrocytes are critical sites of FA oxidation in the CNS (*16*, *17*), indicating their putative involvement in the regulation of energy homeostasis by central lipid homeostasis. Our current results provide a mechanistic explanation for this by showing a bidirectional modulation of astrocytic FA metabolism as core to the vulnerability to HFD-induced obesity. Specifically, we showed that modifications in the astrocytic lipid trafficking affect synaptic tone and activity of POMC neurons via adaptive changes in processes of astrocyte that interact with pre- and postsynaptic elements in hypothalamic neuronal circuits. While we have previously described association between morphological changes of astrocytes and adaptative synaptic changes on hypothalamic neurons (*6*, *7*), in the present study, we showed that astrocyte-specific manipulation of lipid metabolism is sufficient to evoke these circuit alterations. The observed changes in hypothalamic astrocytes in lieu with the changing lipid environment is also reflected in changing mitochondrial dynamics in astrocytes, a result consistent with the role for these adaptive mitochondrial changes in enabling fuel switch (*19*, *20*).

Mitochondria undergo morphological adaptations in response to changes in the metabolic milieu (*19*, *20*, *26*, *35*, *43*). Within the hypothalamus, it has been shown that diet-induced obesity triggers larger and elongated mitochondria in POMC neurons and in microglia (*20*, *44*), whereas in states of negative balance, mitochondria are more numerous, smaller, and rounder in agouti-related protein (AgRP) neurons (*19*). Our current results showed that astrocytic mitochondrial dynamics are controlled by FA availability.

HFD feeding induced increased mitochondria size in hypothalamic astrocytes, which is similar to what we observed regarding mitochondrial adaptations in hypothalamic POMC neurons in response to the same dietary intervention (*20*). We have previously associated these adaptive changes in mitochondrial dynamics with increased carbohydrate availability (*35*). Consistent with this, we found that *Angptl4* mRNA levels are increased in the hypothalamus of HFD-fed mice. Astrocyte-specific knockdown of ANGPTL4 prevented these mitochondrial changes in HFD-fed mice to maintain hypothalamic circuit integrity in support of a lean phenotype. In line with increased FA availability in the hypothalamus of astrocyte-specific ANGPTL4-deficient mice, *Pparγ* mRNA levels were elevated in astrocytes of these animals. In support of the notion that PPARγ signaling is involved in the observed cellular and systemic adaptations to maintain the observed lean phenotype, astrocyte-specific knockdown of PPARγ exacerbated the cellular and whole-body responses to high-fat feeding. While the findings of this study demonstrate the relevance of ANGPTL4 in regulating HFD-induced adaptations of hypothalamic astrocytes and neurons, there are limitations regarding the interpretation of these findings. ANGPTL4 is a secreted protein, and our current work did not determine how the deficiency in astrocytes might influence LPL activity and FA availability in other CNS cellular populations including neurons, microglia, and other cell types. In addition, ANGPTL4 might also regulate intracellular lipolysis, thus controlling FA availability independent of the regulation of LPL activity (*45*). However, recent studies from our laboratory and others using *Angptl4* tissue-specific knockout mouse models have shown that ANGPTL4 have an autocrine role in suppressing LPL activity in vivo (*32*, *36*, *46*). Another experimental observation supporting the autocrine role of ANGPTL4 in astrocytes in regulating glucose homeostasis and obesity was recently provided by Tschöp and colleagues (*5*), who demonstrated that the absence of LPL in astrocytes promotes glucose intolerance, insulin resistance, and obesity. This study demonstrates that the decreased flux of FA into the astrocytes accelerates metabolic dysfunction, which correlates with the opposite phenotype observed in *Angptl4*-deficient mice where the FA uptake should be increased. Collectively, our results revealed a signaling modality whereby astrocytic lipid metabolism affects hypothalamic controllers of feeding, body weight, and systemic glucose regulation, offering an innovative therapeutic target for treatment of metabolic disorders.

MATERIALS AND METHODS

Animal care

All experimental procedures were performed in accordance with the Yale Animal Resources Center and Institutional Animal Care and Use Committee policies. Mice were housed in groups of three to five at 22° to 24°C using a 12-hour light/12-hour dark cycle. Animals had ad libitum access to water and the prescribed diet at all times. Animals were fed a regular chow diet containing 57% calories from carbohydrates, 34% calories from protein, and 9% calories from fat or an HFD containing 35% calories from carbohydrates, 20% calories from protein, and 45% protein from fat (Research Diets, USA). All experiments were performed in adult male and female mice at the age of 8 to 25 weeks. Food intake was assessed weekly. Representative food intake showed in the figures was measured on the last week of chow diet and HFD exposure. Results from males and females are shown separately.

For fasting experiments, mice were allowed to habituate to single-cage housing for 5 days. At the day of experiment, single home cages were changed to avoid mice eating food that may have been deposited in the bedding of the cages. Food was removed from the cages at 3:00 p.m., and mice were euthanized between 8:30 and 9:30 a.m. of the next day.

Tamoxifen administration was carried out as previously described (*7*). Five-week-old mice were injected with tamoxifen (100 mg per kg of body weight, intraperitoneally) for five consecutive days. Exposure to HFD and the metabolic characterization (chow and HFD) started 10 days after the last injection of tamoxifen, allowing the complete removal of *Angptl4* or Pparγ in astrocytes.

Generation of transgenic mice

Angptl4^{GFAP} mice

hGFAP-CreERT2 mice (*7*) were mated with *Angptl4*$^{flox/flox}$ mice (*32*, *36*, *46*), and breeding colonies were maintained by mating *Angptl4*$^{flox/flox}$ females to hGFAP-CreERT2; *Angptl4*$^{flox/flox}$ males. Mice were kept on a 100% C57BL/6 background throughout the experiment. Tamoxifen application at 5 weeks of age as previously described (*7*, *47*) allowed for postnatal deletion of the ANGPTL4 in GFAP-expressing astrocytes (*Angptl4*^{GFAP} mice).

POMC-GFP; Angptl4^{GFAP} mice

Angptl4^{GFAP} mice or *Angptl4*$^{flox/flox}$ mice were mated with POMC–green fluorescent protein (GFP) mice, expressing the GFP in POMC neurons. These mice were generated for electrophysiological purposes. POMC-GFP–positive mice allow the unequivocal identification of POMC cells.

Ppar^{GFAP} mice

hGFAP-CreERT2 mice were mated with *Ppar*$^{flox/flox}$ mice (*40*), and breeding colonies were maintained by mating *Ppar*$^{flox/flox}$ females to hGFAP-CreERT2; *Ppar*$^{flox/flox}$ males. Mice were kept on a 100% C57BL/6 background throughout the experiment.

POMC-GFP; Ppar^{GFAP} mice

Ppar^{GFAP} mice or *Ppar*$^{flox/flox}$ mice were mated with POMC-GFP mice, expressing the GFP in POMC neurons. POMC-GFP–positive mice allow the unequivocal identification of POMC cells.

RPL22; Ppar^{GFAP} mice

Ppar^{GFAP} mice or *Ppar*$^{flox/flox}$ mice were mated with ribosomal protein L22 (RPL22) mice (The Jackson Laboratory), expressing the Rpl22 in a Cre-dependent manner. RPL22 expression allows the study of RNA specifically from GFAP-positive cells.

Glucose tolerance and insulin tolerance tests

Glucose tolerance tests

Glucose tolerance tests (GTTs) were performed in the morning after an overnight fasting period of 16 hours (*8*, *43*). Glucose concentrations in blood were measured from whole venous blood using an automatic glucose monitor (Bayer Contour, Bayer, Germany). After the fasting period, each mouse received an intraperitoneal injection of 20% glucose (2 g/kg body weight; bela-pharm), and blood glucose concentrations were measured before and after 15, 30, 60, and 90 min. GTT was performed on 5- to 6-month-old mice (*8*, *43*).

Insulin tolerance tests

Insulin tolerance tests were performed in the morning in 4-hour fasted mice (*8*, *43*). After determination of basal blood glucose concentrations, each mouse received an intraperitoneal injection of insulin (0.375 U/kg body weight; Insuman Rapid; Sanofi Aventis), and glucose concentrations in the blood were measured after

15, 30, 60, and 90 min. GTT was performed on 5- to 6-month-old mice (*8*, *43*).

β-Gal staining

β-Gal staining was carried out as previously described (*32*, *36*, *46*), ANGPTL4-mutant mice containing a construct with ANGPTL4 exons 4, 5, and 6 flanked by loxP sites and lacZ reporter gene and neomycin resistance gene flanked by flippase recognition target (FRT) sites were generated using a knockout-first strategy and were purchased from the European Conditional Mouse Mutagenesis Program/Knockout Mouse Project (EUCOMM/KOMP) repository. Mice were euthanized, and brains were removed and cut in coronal sections (50 μm). Sections showing different parts of the brain were incubated with β-Gal or β-Gal and anti-GFAP (Sigma-Aldrich). The sections were coverslipped and scoped using a Keyence BZ-X700 fluorescence microscope (*32*, *36*, *46*).

LPL activity assay

Tissue LPL activity was determined as described previously (*32*, *36*, *48*). Briefly, freshly isolated tissues were weighed and homogenized in ice-cold buffer containing phosphate-buffered saline (PBS) with FA-free bovine serum albumin (2 mg/ml), heparin (5 U/ml), 5 mM EDTA, 1% Triton, 0.1% SDS. Homogenates were centrifuged at 3000 rpm for 15 min at 4°C, and supernatant was used for LPL assay. Aliquots (100 ml) of the supenatant were used for the lipase activity assay with 100 ml of 10% intralipid/[3H]-triolein emulsion for 1 hour at 25°C.The activities were normalized for starting tissue weights (*32*, *36*, *48*).

Indirect calorimetry

Indirect calorimetry was performed using an open-circuit, indirect calorimetry system (PhenoMaster, TSE systems) as previously described (*40*, *43*). Briefly, mice were trained for 3 days before data acquisition to adapt to the food/drink dispenser of the PhenoMaster System. Afterward, mice were placed in regular type II cages with sealed lids at room temperature (22°C) and allowed to adapt to the chambers for at least 48 hours. Food and water were provided ad libitum. All parameters were measured continuously and simultaneously (*40*, *43*).

Body composition

Lean and fat mass were analyzed with EchoMRI (EchoMRI LLC, USA) (*43*).

Electron microscopy

Mice (at least four per group) were anesthetized and transcardially perfused with freshly prepared 4% paraformaldehyde and 0.1% glutaraldehyde, as previously reported (*49*–*51*). After postfixation overnight, vibratome sections (50 μm) containing the arcuate nucleus (ARC) were immunostained with primary antibody anti-POMC (dilution 1:7500; H-029-30, Phoenix Pharmaceuticals) or anti-GFAP (dilution 1:4500; Sigma-Aldrich). After overnight incubation at room temperature, sections were washed with phosphate buffer (PB), incubated with biotin-conjugated donkey anti-rabbit immunoglobulin G (IgG) or donkey anti-mouse IgG secondary antibody, respectively (dilution, 1:250; Jackson ImmunoResearch Laboratories), for 2 hours, washed again, put in avidin-biotin complex (Vector Laboratories), and developed with 3,3-diaminobenzidine. Sections were then osmicated (15 min in 1% osmium tetroxide) and dehydrated in increasing ethanol concentrations. During the dehydration, 1% uranyl acetate was added to the 70% ethanol to enhance ultrastructural membrane contrast. Flat embedding in Durcupan followed dehydration. Ultrathin sections were cut on a Leica ultramicrotome, collected on Formvar-coated single-slot grids, and analyzed with a Tecnai 12 Biotwin electron microscope (FEI) with an AMT XR-16 camera (*49*–*51*).

Mitochondria quantification and glia coverage/synaptic inputs analyses

Hypothalamic sections containing POMC or GFAP immunoreactive cells with a visible nucleus were analyzed by electron microscopy. Mitochondrial cross-sectional area, perimeter, and aspect ratio were calculated. Using ImageJ, probability plots were used to estimate changes in mitochondrial size and shape, and statistical differences were tested using the Kolmogorov-Smirnov test. Mitochondrial density was estimated by dividing the number of mitochondrial profiles by the cytosolic or cellular areas. Mitochondrial coverage was estimated by dividing the total area of mitochondria by the cytosolic or cellular areas. Differences in mitochondrial density and coverage were tested using *t* test. For the glia coverage and the synaptic inputs, a blinded investigator scored the number of synapses and the percentage of glia per POMC cell in high magnification images (×>4.800) (*7*, *9*, *51*). $P \leq 0.05$ was considered statistically significant.

Immunofluorescence

Postfixed sections were cut into 50-μm-thick sections. After 15-min washing in PB, the sections were incubated in blocking solution (1:20 normal donkey serum in PBS), containing 0.2% Triton X-100 for 30 min at room temperature. Sections were incubated with anti-GFAP (DAKO), anti-POMC (Phoenix), or a mix of anti-GFAP and anti-cFos (Santa Cruz Biotechnology) overnight at room temperature. The next day, sections were washed three times (5 min) in PB and incubated with the respective secondary antibodies for 1 hour at room temperature [donkey anti-mouse IgG Alexa fluor 594 (dilution, 1:500), donkey anti-chicken IgG Alexa Fluor 488 (dilution, 1:500), and donkey anti-goat 488 (dilution, 1:500); Life Technologies]. The sections were coverslipped and scoped using a Keyence BZ-X700 fluorescence microscope (*49*–*51*).

Astrocyte primary culture

Mice at postnatal day 3 were euthanized by decapitation, and the hypothalamus was collected in Dulbecco's modified Eagle's medium (DMEM) F12 (Gibco) and 1% antibiotics-antimycotics (Gibco) (*7*). The hypothalamus was dissociated, and the suspension was centrifuged for 7 min at 1000 rpm. The pellet was resuspended with DMEM F12 and 10% fetal bovine serum (FBS; Gibco by Life Technologies) and 1% antibiotics-antimycotics. This medium was used to seed and grow cells in 25-cm^3 culture-treated flasks at 37°C and 5% CO_2. The medium was changed every 2 days until it reached the desired confluence. Once confluence was reached, between days 7 and 9 in vitro, the flasks were placed in an incubator shaker at 280 rpm at 37°C overnight. After shaking, the cells were then washed with PBS (Gibco), trypsinized, and resuspended in DMEM F12 plus 10% FBS and 1% antibiotics-antimycotics. The suspension was centrifuged for 5 min at 1150 rpm. After cell counting, the cells were seeded in poly-L-lysine hydrobromide–coated (10 μg/ml; Sigma-Aldrich) six-well plates at a concentration of 130,000 cells per well. The cells were grown for 24 hours in DMEM F12 containing

10% FBS and 1% antibiotics-antimycotics and then treated with palmitic acid (Sigma-Aldrich) or vehicle for 24 hours. Cells were then collected for RNA extraction and polymerase chain reaction (PCR) analysis (*7*).

Analysis of gene expression

RNA was isolated from fresh mediobasal hypothalamic explants using the RNA Micro Kit (Qiagen). RNA was reversely transcribed with the Reverse Transcription Kit (Qiagen) and amplified using the TaqMan Real-Time Master Mix (Roche). All samples were treated with deoxyribonuclease (*49*). Relative expression of target mRNAs was adjusted for total RNA content by *GAPDH* (Mm9999915_91). Inventoried TaqMan probes were used: *Pparγ*, Mm00440939_m1; *Angptl4*, Mm00480431_m1; *Mfn2*, Mm00500120_m1; *GFAP*, Mm01253033_m1; *Cd36*, Mm00432403_m1; *Fasn*, Mm00662319_m1; *Srebp*, Mm00550338_m1; and *Accalpha*, Mm01304258_m1 (Thermo Fisher Scientific). Calculations were performed by a comparative method ($2^{-\Delta\Delta CT}$). Quantitative PCR was performed on aLightCycler 480 (Roche) (*49*).

Ribosomal profiling

Translating ribosome affinity purification was conducted in homogenate samples of MBH obtained from mice with loxP-flanked Rpl22 crossed with the $Angptl4^{GFAP}$ or $Ppar^{GFAP}$ mice lines, which express Rpl22 and hemagglutinin proteins in ribosomes of astrocytes, thereby allowing for the immunoprecipitation of polysomes directly from GFAP-positive astrocytes (*7*, *51*). After RNA isolation, we obtained approximately 10 to 25 ng of RNA per sample. Reverse transcription PCR was performed as described above.

Western blotting

Mice were euthanized, and the MBH was extracted. Protein was extracted using radioimmunoprecipitation assay buffer containing Compete Protease Inhibitor Cocktail (Roche, USA). Proteins were transferred on polyvinylidene difluoride membranes using a Trans Blot Turbo transfer apparatus (Bio-Rad, Hercules, CA, USA) and incubated with anti-GFAP (Dako; 1:1000), AMPK (MP-activated protein kinase), pAMPK, ACC (acetyl-CoA carboxylase), pACC, CD36, pHSL (phoshorylated hormone-sensitive lipase) (Cell Signaling Technology), and anti–glyceraldehyde-3-phosphate dehydrogenase (Calbiochem; 1:10,000). Detection was carried out using enhanced chemiluminescence (Bio-Rad) (*49*, *51*).

Electrophysiology

The coronal hypothalamic slices containing the ARC were prepared from $Angptl4^{GFAP}$, $Ppar^{GFAP}$ mice and their respective controls, as previously reported (*49*–*51*). Briefly, mice were anesthetized with isoflurane and decapitated, and the brain was rapidly removed and immersed in a cold (4°C) and oxygenated cutting solution containing the following: 220 mM sucrose, 2.5 mM KCl, 1.23 mM NaH_2PO_4, 26 mM $NaHCO_3$, 1 mM $CaCl_2$, 6 mM $MgCl_2$, and 10 mM glucose (pH 7.3 with NaOH). Coronal hypothalamic slices (300 μm thick) were prepared with a Leica vibratome after the brain was trimmed to a small tissue block containing the hypothalamus. After preparation, slices were maintained at room temperature (23° to 25°C) in a storage chamber in the artificial cerebrospinal fluid (ACSF) (bubbled with 5% CO_2 and 95% O_2) containing the following: 124 mM NaCl, 3 mM KCl, 2 mM $CaCl_2$, 2 mM $MgCl_2$, 1.23 mM NaH_2PO_4, 26 mM $NaHCO_3$, and 10 mM glucose (pH 7.4 with NaOH), for recovery and storage. After recovery at room temperature for at least 1 hour, slices were transferred to a recording chamber constantly perfused at a rate of 2 ml/min with ACSF containing 2.5 mM glucose at a temperature of 33°C for electrophysiological experiments. Whole-cell patch-clamp recording was performed in POMC-GFP–positive cells, and spontaneous membrane (MP) was recorded under a current clamp. The micropipettes (4 to 6 megohm) were made of borosilicate glass (World Precision Instruments) with a micropipette puller (Sutter P-97) and back-filled with a pipette solution containing the following: 108 mM K-gluconate, 27 mM KCl, 2 mM $MgCl_2$, 10 mM Hepes, 1.1 mM EGTA, 2.5 mM Mg-ATP, 0.3 mM Na_2-GTP, and 10 mM Na_2-phosphocreatin (pH 7.3 with KOH). Both input resistance and series resistance were monitored throughout the experiments, and the former was partially compensated. Only recordings with stable series resistance and input resistance were accepted. All data were sampled at 3 kHz, filtered at 3 kHz, and analyzed with an Apple Macintosh computer using Axograph X (AxoGraph). *T* test was used to examine the statistical significance of the difference in MP in the recorded glial cells (*49*–*51*).

Statistical analyses

Statistical analyses were performed with Prism 8 (GraphPad). All data are expressed as the means ± SEM. Comparisons for two groups were calculated using unpaired two-tailed Student's *t* tests, one-way analysis of variance (ANOVA) followed by Bonferroni's multiple comparison tests for more than two groups, and two-way ANOVA for experiments with more than two variants followed by multiple comparison. For analyses of populations (cumulative distributions), Kolmogorov-Smirnov test was used. Significance for all analyses was taken at $^{*}P < 0.05$, $^{**}P < 0.01$, and $^{***}P < 0.001$. Shapiro-Wilk normality test was used to assess the Gaussian distribution of each dataset. All datasets show normal distribution.

SUPPLEMENTARY MATERIALS

Supplementary material for this article is available at https://science.org/doi/10.1126/sciadv.abj2814

View/request a protocol for this paper from *Bio-protocol*.

REFERENCES AND NOTES

1. A. Araque, Astrocytes process synaptic information. *Neuron Glia Biol.* **4**, 3–10 (2008).
2. H. G. Bernstein, J. Steiner, B. Bogerts, Glial cells in schizophrenia: Pathophysiological significance and possible consequences for therapy. *Expert Rev. Neurother.* **9**, 1059–1071 (2009).
3. R. J. Kelleher, R. L. Soiza, Evidence of endothelial dysfunction in the development of Alzheimer's disease: Is Alzheimer's a vascular disorder? *Am. J. Cardiovasc. Dis.* **3**, 197–226 (2013).
4. E. Kobayashi, M. Nakano, K. Kubota, N. Himuro, S. Mizoguchi, T. Chikenji, M. Otani, Y. Mizue, K. Nagaishi, M. Fujimiya, Activated forms of astrocytes with higher GLT-1 expression are associated with cognitive normal subjects with Alzheimer pathology in human brain. *Sci. Rep.* **8**, 1712 (2018).
5. Y. Gao, C. Layritz, B. Legutko, T. O. Eichmann, E. Laperrousaz, V. S. Moulle, C. Cruciani-Guglielmacci, C. Magnan, S. Luquet, S. C. Woods, R. H. Eckel, C. X. Yi, C. Garcia-Caceres, M. H. Tschöp, Disruption of lipid uptake in astroglia exacerbates diet-induced obesity. *Diabetes* **66**, 2555–2563 (2017).
6. T. L. Horvath, B. Sarman, C. Garcia-Caceres, P. J. Enriori, P. Sotonyi, M. Shanabrough, E. Borok, J. Argente, J. A. Chowen, D. Perez-Tilve, P. T. Pfluger, H. S. Bronneke, B. E. Levin, S. Diano, M. A. Cowley, M. H. Tschop, Synaptic input organization of the melanocortin system predicts diet-induced hypothalamic reactive gliosis and obesity. *Proc. Natl. Acad. Sci. U.S.A.* **107**, 14875–14880 (2010).
7. J. G. Kim, S. Suyama, M. Koch, S. Jin, P. Argente-Arizon, J. Argente, Z. W. Liu, M. R. Zimmer, J. K. Jeong, K. Szigeti-Buck, Y. Gao, C. Garcia-Caceres, C. X. Yi, N. Salmaso, F. M. Vaccarino, J. Chowen, S. Diano, M. O. Dietrich, M. H. Tschop, T. L. Horvath, Leptin signaling

in astrocytes regulates hypothalamic neuronal circuits and feeding. *Nat. Neurosci.* **17**, 908–910 (2014).
8. K. Timper, A. Del Río-Martin, A. L. Cremer, S. Bremser, J. Alber, P. Giavalisco, L. Varela, C. Heilinger, H. Nolte, A. Trifunovic, T. L. Horvath, P. Kloppenburg, H. Backes, J. C. Bruning, GLP-1 receptor signaling in astrocytes regulates fatty acid oxidation, mitochondrial integrity, and function. *Cell Metab.* **31**, 1189–1205.e13 (2020).
9. C. Garcia-Caceres, C. Quarta, L. Varela, Y. Gao, T. Gruber, B. Legutko, M. Jastroch, P. Johansson, J. Ninkovic, C. X. Yi, O. Le Thuc, K. Szigeti-Buck, W. Cai, C. W. Meyer, P. T. Pfluger, A. M. Fernandez, S. Luquet, S. C. Woods, I. Torres-Aleman, C. R. Kahn, M. Gotz, T. L. Horvath, M. H. Tschop, Astrocytic insulin signaling couples brain glucose uptake with nutrient availability. *Cell* **166**, 867–880 (2016).
10. L. Varela, B. Stutz, J. E. Song, J. G. Kim, Z. W. Liu, X. B. Gao, T. L. Horvath, Hunger-promoting AgRP neurons trigger an astrocyte-mediated feed-forward auto-activation loop in mice. *J. Clin. Invest.* **131**, e144239 (2021).
11. D. Cota, K. Proulx, K. A. Smith, S. C. Kozma, G. Thomas, S. C. Woods, R. J. Seeley, Hypothalamic mTOR signaling regulates food intake. *Science* **312**, 927–930 (2006).
12. M. J. Wolfgang, M. D. Lane, Hypothalamic malonyl-coenzyme A and the control of energy balance. *Mol. Endocrinol.* **22**, 2012–2020 (2008).
13. Y. Minokoshi, T. Alquier, N. Furukawa, Y. B. Kim, A. Lee, B. Xue, J. Mu, F. Foufelle, P. Ferre, M. J. Birnbaum, B. J. Stuck, B. B. Kahn, AMP-kinase regulates food intake by responding to hormonal and nutrient signals in the hypothalamus. *Nature* **428**, 569–574 (2004).
14. L. Varela, N. Martinez-Sanchez, R. Gallego, M. J. Vazquez, J. Roa, M. Gandara, E. Schoenmakers, R. Nogueiras, K. Chatterjee, M. Tena-Sempere, C. Dieguez, M. Lopez, Hypothalamic mTOR pathway mediates thyroid hormone-induced hyperphagia in hyperthyroidism. *J. Pathol.* **227**, 209–222 (2012).
15. Z. B. Andrews, Z. W. Liu, N. Walllingford, D. M. Erion, E. Borok, J. M. Friedman, M. H. Tschop, M. Shanabrough, G. Cline, G. I. Shulman, A. Coppola, X. B. Gao, T. L. Horvath, S. Diano, UCP2 mediates ghrelin's action on NPY/AgRP neurons by lowering free radicals. *Nature* **454**, 846–851 (2008).
16. P. Schönfeld, G. Reiser, Why does brain metabolism not favor burning of fatty acids to provide energy? Reflections on disadvantages of the use of free fatty acids as fuel for brain. *J. Cereb. Blood Flow Metab.* **33**, 1493–1499 (2013).
17. C. Le Foll, B. E. Levin, Fatty acid-induced astrocyte ketone production and the control of food intake. *Am. J. Phys. Regul. Integr. Comp. Phys.* **310**, R1186–R1192 (2016).
18. A. Santoro, M. Campolo, C. Liu, H. Sesaki, R. Meli, Z. W. Liu, J. D. Kim, S. Diano, DRP1 suppresses leptin and glucose sensing of POMC neurons. *Cell Metab.* **25**, 647–660 (2017).
19. M. O. Dietrich, Z. W. Liu, T. L. Horvath, Mitochondrial dynamics controlled by mitofusins regulate Agrp neuronal activity and diet-induced obesity. *Cell* **155**, 188–199 (2013).
20. M. Schneeberger, M. O. Dietrich, D. Sebastian, M. Imbernon, C. Castano, A. Garcia, Y. Esteban, A. Gonzalez-Franquesa, I. C. Rodriguez, A. Bortolozzi, P. M. Garcia-Roves, R. Gomis, R. Nogueiras, T. L. Horvath, A. Zorzano, M. Claret, Mitofusin 2 in POMC neurons connects ER stress with leptin resistance and energy imbalance. *Cell* **155**, 172–187 (2013).
21. G. Mancini, K. Pirruccio, X. Yang, M. Bluher, M. Rodeheffer, T. L. Horvath, Mitofusin 2 in mature adipocytes controls adiposity and body weight. *Cell Rep.* **26**, 2849–2858.e4 (2019).
22. D. Sebastian, M. I. Hernandez-Alvarez, J. Segales, E. Sorianello, J. P. Munoz, D. Sala, A. Waget, M. Liesa, J. C. Paz, P. Gopalacharyulu, M. Oresic, S. Pich, R. Burcelin, M. Palacin, A. Zorzano, Mitofusin 2 (Mfn2) links mitochondrial and endoplasmic reticulum function with insulin signaling and is essential for normal glucose homeostasis. *Proc. Natl. Acad. Sci. U.S.A.* **109**, 5523–5528 (2012).
23. H. F. Jheng, P. J. Tsai, S. M. Guo, L. H. Kuo, C. S. Chang, I. J. Su, C. R. Chang, Y. S. Tsai, Mitochondrial fission contributes to mitochondrial dysfunction and insulin resistance in skeletal muscle. *Mol. Cell. Biol.* **32**, 309–319 (2012).
24. A. J. A. Molina, J. D. Wikstrom, L. Stiles, G. Las, H. Mohamed, A. Elorza, G. Walzer, G. Twig, S. Katz, B. E. Corkey, O. S. Shirihai, Mitochondrial networking protects β-cells from nutrient-induced apoptosis. *Diabetes* **58**, 2303–2315 (2009).
25. J. E. Song, T. C. Alves, B. Stutz, M. Sestan-Pesa, N. Kilian, S. Jin, S. Diano, R. G. Kibbey, T. L. Horvath, Mitochondrial fission governed by Drp1 regulates exogenous fatty acid usage and storage in hela cells. *Metabolites* **11**, 322 (2021).
26. M. Liesa, O. S. Shirihai, Mitochondrial dynamics in the regulation of nutrient utilization and energy expenditure. *Cell Metab.* **17**, 491–506 (2013).
27. S. Kersten, S. Mandard, N. S. Tan, P. Escher, D. Metzger, P. Chambon, F. J. Gonzalez, B. Desvergne, W. Wahli, Characterization of the fasting-induced adipose factor FIAF, a novel peroxisome proliferator-activated receptor target gene. *J. Biol. Chem.* **275**, 28488–28493 (2000).
28. V. Sukonina, A. Lookene, T. Olivecrona, G. Olivecrona, Angiopoietin-like protein 4 converts lipoprotein lipase to inactive monomers and modulates lipase activity in adipose tissue. *Proc. Natl. Acad. Sci. U.S.A.* **103**, 17450–17455 (2006).
29. R. Zhang, The ANGPTL3-4-8 model, a molecular mechanism for triglyceride trafficking. *Open Biol.* **6**, 150272 (2016).
30. B. Aryal, N. L. Price, Y. Suarez, C. Fernandez-Hernando, ANGPTL4 in metabolic and cardiovascular disease. *Trends Mol. Med.* **25**, 723–734 (2019).
31. B. Aryal, N. Rotllan, E. Araldi, C. M. Ramirez, S. He, B. G. Chousterman, A. M. Fenn, A. Wanschel, J. Madrigal-Matute, N. Warrier, J. L. Martin-Ventura, F. K. Swirski, Y. Suarez, C. Fernandez-Hernando, ANGPTL4 deficiency in haematopoietic cells promotes monocyte expansion and atherosclerosis progression. *Nat. Commun.* **7**, 12313 (2016).
32. B. Aryal, A. K. Singh, X. Zhang, L. Varela, N. Rotllan, L. Goedeke, B. Chaube, J. P. Camporez, D. F. Vatner, T. L. Horvath, G. I. Shulman, Y. Suarez, C. Fernandez-Hernando, Absence of ANGPTL4 in adipose tissue improves glucose tolerance and attenuates atherogenesis. *JCI Insight* **3**, e97918 (2018).
33. H. K. Kim, B. S. Youn, M. S. Shin, C. Namkoong, K. H. Park, J. H. Baik, J. B. Kim, J. Y. Park, K. U. Lee, Y. B. Kim, M. S. Kim, Hypothalamic Angptl4/Fiaf is a novel regulator of food intake and body weight. *Diabetes* **59**, 2772–2780 (2010).
34. S. G. Vienberg, A. Kleinridders, R. Suzuki, C. R. Kahn, Differential effects of angiopoietin-like 4 in brain and muscle on regulation of lipoprotein lipase activity. *Mol. Metab.* **4**, 144–150 (2015).
35. C. M. Nasrallah, T. L. Horvath, Mitochondrial dynamics in the central regulation of metabolism. *Nat. Rev. Endocrinol.* **10**, 650–658 (2014).
36. A. K. Singh, B. Aryal, B. Chaube, N. Rotllan, L. Varela, T. L. Horvath, Y. Suarez, C. Fernandez-Hernando, Brown adipose tissue derived ANGPTL4 controls glucose and lipid metabolism and regulates thermogenesis. *Mol. Metab.* **11**, 59–69 (2018).
37. L. La Paglia, A. Listi, S. Caruso, V. Amodeo, F. Passiglia, V. Bazan, D. Fanale, Potential role of ANGPTL4 in the cross talk between metabolism and cancer through PPAR signaling pathway. *PPAR Res.* **2017**, 8187235 (2017).
38. F. E. Dewey, V. Gusarova, C. O'Dushlaine, O. Gottesman, J. Trejos, C. Hunt, C. V. Van Hout, L. Habegger, D. Buckler, K. M. Lai, J. B. Leader, M. F. Murray, M. D. Ritchie, H. L. Kirchner, D. H. Ledbetter, J. Penn, A. Lopez, I. B. Borecki, J. D. Overton, J. G. Reid, D. J. Carey, A. J. Murphy, G. D. Yancopoulos, A. Baras, J. Gromada, A. R. Shuldiner, Inactivating variants in ANGPTL4 and risk of coronary artery disease. *N. Engl. J. Med.* **374**, 1123–1133 (2016).
39. L. Lichtenstein, F. Mattijssen, N. J. de Wit, A. Georgiadi, G. J. Hooiveld, R. van der Meer, Y. He, L. Qi, A. Koster, J. T. Tamsma, N. S. Tan, M. Muller, S. Kersten, Angptl4 protects against severe proinflammatory effects of saturated fat by inhibiting fatty acid uptake into mesenteric lymph node macrophages. *Cell Metab.* **12**, 580–592 (2010).
40. L. Long, C. Toda, J. K. Jeong, T. L. Horvath, S. Diano, PPARγ ablation sensitizes proopiomelanocortin neurons to leptin during high-fat feeding. *J. Clin. Invest.* **124**, 4017–4027 (2014).
41. S. Diano, Z. W. Liu, J. K. Jeong, M. O. Dietrich, H. B. Ruan, E. Kim, S. Suyama, K. Kelly, E. Gyengesi, J. L. Arbiser, D. D. Belsham, D. A. Sarruf, M. W. Schwartz, A. M. Bennett, M. Shanabrough, C. V. Mobbs, X. Yang, X. B. Gao, T. L. Horvath, Peroxisome proliferation-associated control of reactive oxygen species sets melanocortin tone and feeding in diet-induced obesity. *Nat. Med.* **17**, 1121–1127 (2011).
42. T. L. Horvath, Z. B. Andrews, S. Diano, Fuel utilization by hypothalamic neurons: Roles for ROS. *Trends Endocrinol. Metab.* **20**, 78–87 (2009).
43. C. Toda, J. D. Kim, D. Impellizzeri, S. Cuzzocrea, Z. W. Liu, S. Diano, UCP2 regulates mitochondrial fission and ventromedial nucleus control of glucose responsiveness. *Cell* **164**, 872–883 (2016).
44. J. D. Kim, N. A. Yoon, S. Jin, S. Diano, Microglial UCP2 mediates inflammation and obesity induced by high-fat feeding. *Cell Metab.* **30**, 952–962.e5 (2019).
45. A. E. McQueen, D. Kanamaluru, K. Yan, N. E. Gray, L. Wu, M. L. Li, A. Chang, A. Hasan, D. Stifler, S. K. Koliwad, J. C. Wang, The C-terminal fibrinogen-like domain of angiopoietin-like 4 stimulates adipose tissue lipolysis and promotes energy expenditure. *J. Biol. Chem.* **292**, 16122–16134 (2017).
46. A. K. Singh, B. Chaube, X. Zhang, J. Sun, K. M. Citrin, A. Canfrán-Duque, B. Aryal, N. Rotllan, L. Varela, R. G. Lee, T. L. Horvath, N. Price, Y. Suarez, C. Fernandez-Hernando, Hepatocyte-specific suppression of ANGPTL4 improves obesity-associated diabetes and mitigates atherosclerosis in mice. *J. Clin. Invest.* **131**, e140989 (2021).
47. L. Koch, F. T. Wunderlich, J. Seibler, A. C. Konner, B. Hampel, S. Irlenbusch, G. Brabant, C. R. Kahn, F. Schwenk, J. C. Bruning, Central insulin action regulates peripheral glucose and fat metabolism in mice. *J. Clin. Invest.* **118**, 2132–2147 (2008).
48. P. L. S. M. Gordts, R. Nock, N.-H. Son, B. Ramms, I. Lew, J. C. Gonzales, B. E. Thacker, D. Basu, R. G. Lee, A. E. Mullick, M. J. Graham, I. J. Goldberg, R. M. Crooke, J. L. Witztum, J. D. Esko, ApoC-III inhibits clearance of triglyceride-rich lipoproteins through LDL family receptors. *J. Clin. Invest.* **126**, 2855–2866 (2016).
49. L. Varela, S. Suyama, Y. Huang, M. Shanabrough, M. H. Tschop, X. B. Gao, F. J. Giordano, T. L. Horvath, Endothelial HIF-1α enables hypothalamic glucose uptake to drive POMC neurons. *Diabetes* **66**, 1511–1520 (2017).
50. M. Koch, L. Varela, J. G. Kim, J. D. Kim, F. Hernandez-Nuno, S. E. Simonds, C. M. Castorena, C. R. Vianna, J. K. Elmquist, Y. M. Morozov, P. Rakic, I. Bechmann, M. A. Cowley,

K. Szigeti-Buck, M. O. Dietrich, X. B. Gao, S. Diano, T. L. Horvath, Hypothalamic POMC neurons promote cannabinoid-induced feeding. *Nature* **519**, 45–50 (2015).
51. L. Varela, B. Stutz, J. E. Song, J. G. Kim, Z. W. Liu, X. B. Gao, T. L. Horvath, Hunger-promoting AgRP neurons trigger an astrocyte-mediated feed-forward autoactivation loop in mice. *J. Clin. Invest.* **131**, e144239 (2021).

Acknowledgments
Funding: This work was supported by National Institutes of Health grant AG052005 (T.L.H.), National Institutes of Health grant AG067329 (T.L.H.), National Institutes of Health grant DK126447 (T.L.H.), The Klarman Family Foundation (T.L.H.), and National Institutes of Health grant R35HL135820 (C.F.-H.). **Author contributions:** L.V., J.G.K., P.F.-T., B.A., and Z.W.L. performed the experiments. L.V. and T.L.H. designed the study. L.V., C.F.-H., and T.L.H. wrote and edited the manuscript. **Competing interests:** The authors declare that they have no competing interests. **Data and materials availability:** All data needed to evaluate the conclusions in the paper are present in the paper and/or the Supplementary Materials.

Submitted 3 May 2021
Accepted 22 October 2021
Published 10 December 2021
10.1126/sciadv.abj2814